Microtribological and Nanomechanical Properties of Switchable Y-Shaped Amphiphilic Polymer Brushes**

By *Melburne C. LeMieux*, *Yen-Hsi Lin*, *Pham Duc Cuong*, *Hyo-Sok Ahn*,* *Eugene R. Zubarev*, and *Vladimir V. Tsukruk**

We have characterized the morphology and nanomechanical properties of surface-grafted nanoscale layers consisting of Y-shaped binary molecules with one polystyrene (PS) arm and one poly(acrylic acid) (PAA) arm. We examined these amphiphilic brushes in fluids (in-situ visualization), and measured their microtribological characteristics as a function of chemical composition. Atomic force microscopy (AFM)-based nanomechanical testing has shown that nanoscale reorganization greatly influences the adhesion and elastic properties of the nanoscale brush layer. In water, a bimodal distribution of the elastic modulus, arising from the mixed chemical composition of the topmost layer, is observed. In contrast, the top layer is completely dominated by PS in toluene. As a result of this reorganization, the Y-shaped-brush layer exhibits a dramatic variation in the friction and wear properties after exposure to different solvents. Unexpectedly, the tribological properties are enhanced for the hydrophilic and polar, PAA-dominated, surface, which shows a lower friction coefficient and higher wear stability, despite higher adhesion and heterogeneous surface composition. We suggest that this unusual behavior is caused by the combination of the presence of a thicker water layer on the PAA-enriched surface that acts as a boundary lubricant and the glassy state of the PAA chains.

1. Introduction

Numerous examples of polymer brushes reported in the literature clearly demonstrate the potential of brushes for creating a new generation of materials, the properties of which could be tuned in a reversible manner upon changes in the local environment.[1] External stimuli, such as subtle changes in chemical species,[2] pH,[3] temperature,[4] pressure,[5] and light,[6] on interaction with a polymer brush have been shown to dramatically change its surface morphology, composition, and properties. Brushes based on block copolymers covalently attached to solid substrates,[7] as well as mixed brushes,[8] are particularly intriguing examples in that respect, because a large variety of surface morphologies is possible. Surface composition, and hence properties such as surface energy, adhesion, friction, and wettability, have the possibility of being "tuned" to the required state.[9]

The interplay of interchain interactions and the penalty of entropic elasticity leads to lateral phase separation and a characteristic "rippled" morphology, as was initially predicted by theory[10,11] and later confirmed experimentally.[8c,12] The presence of a solvent that is selective for a particular part of the brush was observed to cause significant conformational rearrangements and the solvent–brush interactions promoted "perpendicular" microphase separation;[13] in this case, the top layer composed of soluble chains covered collapsed insoluble blocks. Thus, the morphology of a given brush, owing to the high grafting density and uniformity in thickness and morphology, may undergo remarkable changes upon the smallest fluctuations in solvent conditions. In fact, recent studies by Möller and co-workers have shown that even the presence of solvent vapor can change the shape of brush-like macromolecules from an extended worm-like conformation to a compact globule, and vice versa.[14]

The morphology of block-copolymer brushes also depends on the particular point at which the macromolecule is tethered to the substrate. Several researchers predicted the formation of many unusual morphologies and nanopatterns if a block copolymer were to be attached to a solid surface through its junction point, the point that connects two incompatible blocks.[15,16] Such Y-shaped macromolecules were later synthesized[17] and successfully grafted to silicon substrates, as described elsewhere.[18,19] We observed a unique "crater-like" morphology that could be switched reversibly to "pinned micellar" structures after amphiphilic polystyrene–poly(acrylic acid) (PS-PAA) brushes were treated with particular solvents.[18,19] However, the fundamental question remained: do the same morphologies exist in the presence of different selective solvents? In our preliminary report, we described the conditions for atomic force microscopy (AFM) imaging of a PS_{40}-PAA_{30} Y-shaped brush in fluids, but how the observed

[*] Prof. V. V. Tsukruk, M. C. LeMieux, Y.-H. Lin, Prof. E. R. Zubarev
Department of Materials Science and Engineering
Iowa State University
2220 Hoover Hall, Ames, IA 50011 (USA)
E-mail: Vladimir@iastate.edu
Prof. H.-S. Ahn, P. D. Cuong
Tribology Research Center
Korean Institute of Science and Technology
39-1 Hawolgok-dong, Songbuk-gu, Seoul 136-791 (Korea)
E-mail: hsahn@kist.re.kr

[**] This research was supported by the National Science Foundation through grants CMS-0099868 and DMR-0308982. E.R.Z. is grateful to the American Chemical Society Petroleum Research Fund for partial support of this research (ACS-PRF No. 40727 G-10).

 DOI: 10.1002/adfm.200500088

morphological changes affect engineering properties, such as mechanical and tribological properties, was not revealed.[20] These covalently bound nanoscale layers show a dramatic switching of morphology and surface roughness by sensing the local environment. Because of this, they have great potential as prospective materials in microfluidic devices that require "smart" surfaces, as well as for controlling the adsorption of proteins or inorganic nanoparticles, especially as a result of our design approach of switching between a sticky hydrophilic surface and a repellent hydrophobic surface layer. In general, this report addresses a largely unexplored field, that of characterizing the properties of switchable polymer layers *directly in* a fluid. Such knowledge is imperative because the applications listed above, and most of the foreseen applications of polymer nanolayers, especially in biotechnological and microfluidic fields, involve implementing them in fluid environments.

Herein, we explore how the chemical composition of the Y-shaped molecules chemically grafted to a silicon surface affects the morphology, microroughness, adhesion, and elastic modulus *in the presence* of selective solvents. In addition, we report the unique measurements of the microtribological properties of the Y-shaped brush layers in which the frictional forces and wear were found to depend strongly on the morphology and composition of the brush layer, with much better wear stability unexpectedly found for the more polar layer with mixed chemical composition. Microtribological properties may be reversibly tuned by solvent treatment.

2. Results and Discussion

2.1. Surface Morphology of Amphiphilic Y-Brushes in Selective Solvents

Upon grafting, the Y-shaped molecules formed a clean, homogeneous surface with a surface microroughness below 0.4 nm in the dry state. This value of surface roughness, measured over a 1 μm × 1 μm area, was far below the contour length of both the PAA and PS arms, which ranged from 25 to 40 monomeric units (6–10 nm), respectively, implying that the grafted layers exhibit molecular smoothness. The dry thickness of the PS-PAA-grafted layer was 1.4 and 1.9 ± 0.2 nm for **Y1** (PS_{40}-PAA_{30}, Fig. 1) and **Y2** (PS_{25}-PAA_{25}, Fig. 1), respectively (Table 1), as measured independently via ellipsometry and AFM scratch tests. The medium grafting density (Table 1), typical of the "grafting-to" approach, corresponds to a distance of 3.5 nm between the anchor locations of the Y-shape molecules. This indicates the arms are slightly deformed (constrained), as is typical for a brush regime.[21] The effect of PS versus PAA composition in **Y1** and **Y2** was observed via contact-angle measurements after treatment with toluene. Brushes based on molecule **Y1** have a contact angle of 73°; the symmetric **Y2** brush has a contact angle of 61° (Table 1). The lower value of **Y2** is a reflection of a lower composition of the hydrophobic PS chains at the surface compared to **Y1** brushes.

The morphology of the grafted layers was characterized using in-situ AFM under toluene and water (Fig. 2). The thickness of the brushes in each solvent measured by the AFM scratch tests in fluid averaged 5.5 ± 0.5 nm for all surfaces, as demonstrated for the **Y1**-brush layer with cross-sections obtained directly in each solvent (Figs. 2a,b). This is nearly four times higher than for the dry-state thickness (Table 1), and represents a typical brush-like state in which the chains swell away from the surface owing to entropic effects and the resulting osmotic pressure. Owing to the extremely small size of the structural features in these layers, from the 1 μm × 1 μm AFM images alone it remains unclear whether or not the brush is switching between a topmost layer dominated by PS blocks in toluene and a PAA-dominated top layer under water. However, there are rather significant differences in the roughness of the brushes measured in toluene and in water, which can be observed in the high-resolution three-dimensional images presented in Figure 3. Notably, the roughness measured by AFM is two to three times higher in water than in toluene (Table 2).

In water, the hydrophobic PS chains of **Y1** cannot be covered completely by PAA, as its volume fraction is nearly half that of the bulky PS arms (34 vs. 66 %). A similar observation was made for **Y2**, although the volume fraction of PAA chains in this brush is slightly lower (30 %), causing an even larger disparity in coverage. The layering of PAA over the PS arms is incomplete in both brushes in water, leading to higher heterogeneity and surface microroughness. On the other hand, in toluene, which is a good solvent for PS, the surface roughness is lower, suggesting that a more homogenous top layer is present. In fact, longer PS arms can shield the layer of collapsed PAA chains, which have a lower volume fraction and a greater affinity for the hydrophilic silicon substrate.

Molecular modeling of the Y-shaped PS-PAA brushes explains the observed switching of the morphology (Fig. 3). We modeled seven Y-shaped molecules on a hexagonal lattice spaced 3.5 nm apart, which represents an experimentally determined distance between the anchor points. Using a force-field minimization and taking the factors described above into account, the model revealed a more vertical layering of PS over PAA in toluene (Fig. 3), producing a continuous PS surface. On the other hand, owing to the lower extent of PS collapse in water, the PAA arms cannot form a complete homogeneous layer over PS, thereby forming the crater-like structure similar to that observed in the dry state.[19] However, this morphology is more amplified in the presence of a selective solvent, as in water the hydrophilic PAA chains stretch out in a direction perpendicular to the surface. This crater-like morphology is responsible for the three-fold increase in the surface microroughness as the brush is transferred from a toluene to an aqueous environment. These data demonstrate the high switchability of this important parameter, and the stimuli-responsive nature of the Y-shaped amphiphilic brushes (Table 2).

ADVANCED FUNCTIONAL MATERIALS

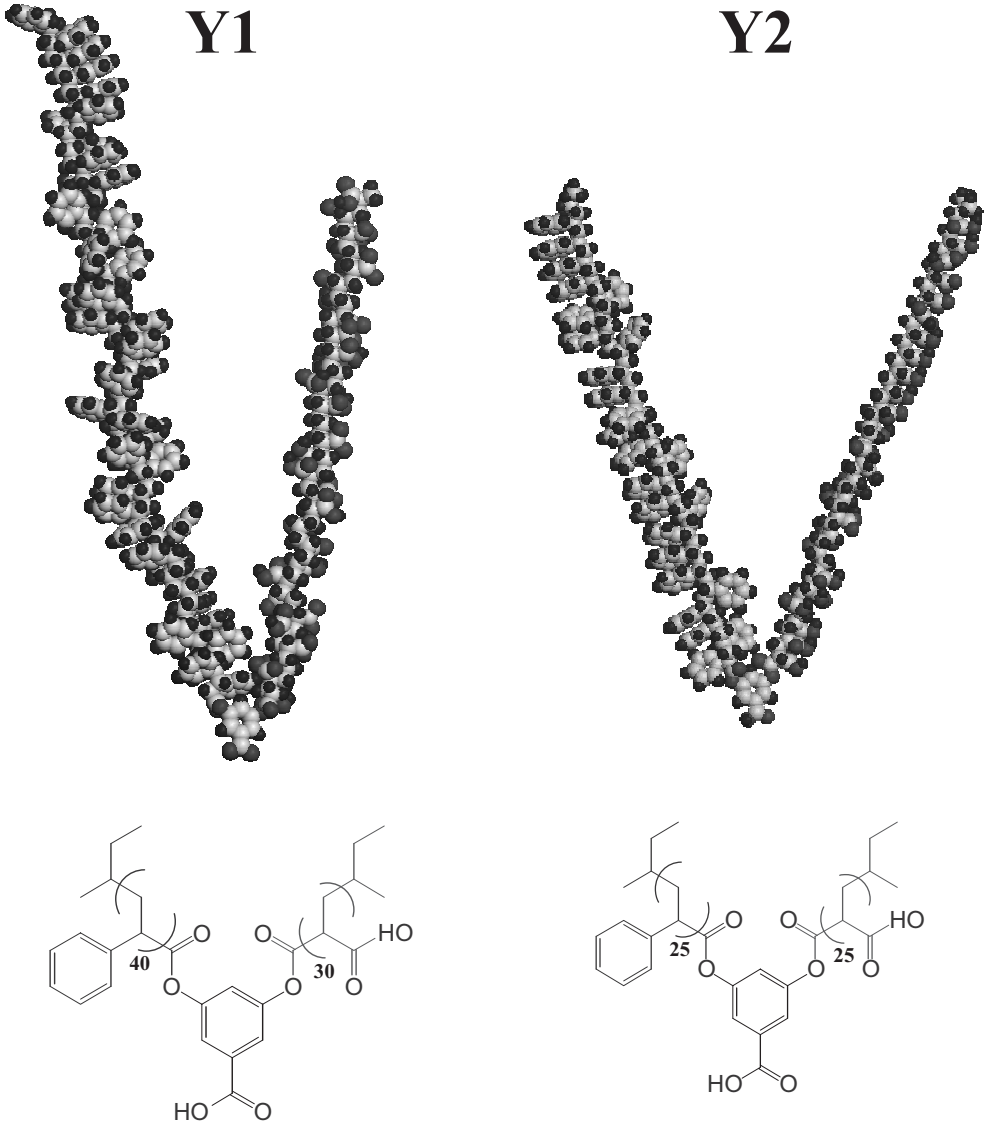

Figure 1. Molecular models and chemical structures of the **Y1** and **Y2** arms, and the short anchoring junction (functional aromatic group). **Y1** consists of 40 PS and 30 PAA monomeric units; **Y2** is symmetrical with 25 units of each.

Table 1. Parameters of the Y-shaped PS-PAA grafted layers in air.

Brush	As-synthesized thickness [nm]	Microroughness [nm]	Contact angle [°]		Grafted amount [mg m^{-2}]	Grafting density [chains nm^{-2}]
			After water	After toluene		
Y1	1.4 ± 0.20	0.37 ± 0.1	54 ± 2	73 ± 2	1.42	0.11
Y2	1.9 ± 0.22	0.27 ± 0.1	50 ± 2	61 ± 2	1.95	0.20

Table 2. Physical properties of the Y-shaped layers in different solvents. (μ: Friction coefficient.)

Brush/Environment	Microroughness [nm]	Average stable μ [a]	Normalized pull-off force [pN nm^{-1}]	Elastic modulus [MPa]
Y1 in toluene	0.44 ± 0.2	0.35	< 0.5	4.6
Y1 in water	0.73 ± 0.3	0.21	20	Crater rim: 4.3 Crater pit: 110
Y2 in toluene	0.27 ± 0.1	0.55	< 0.5	22
Y2 in water	0.90 ± 0.1	0.35	39	Crater rim: 2.2 Crater pit: 125

[a] Tested in the dry state, after exposure to the respective solvent listed.

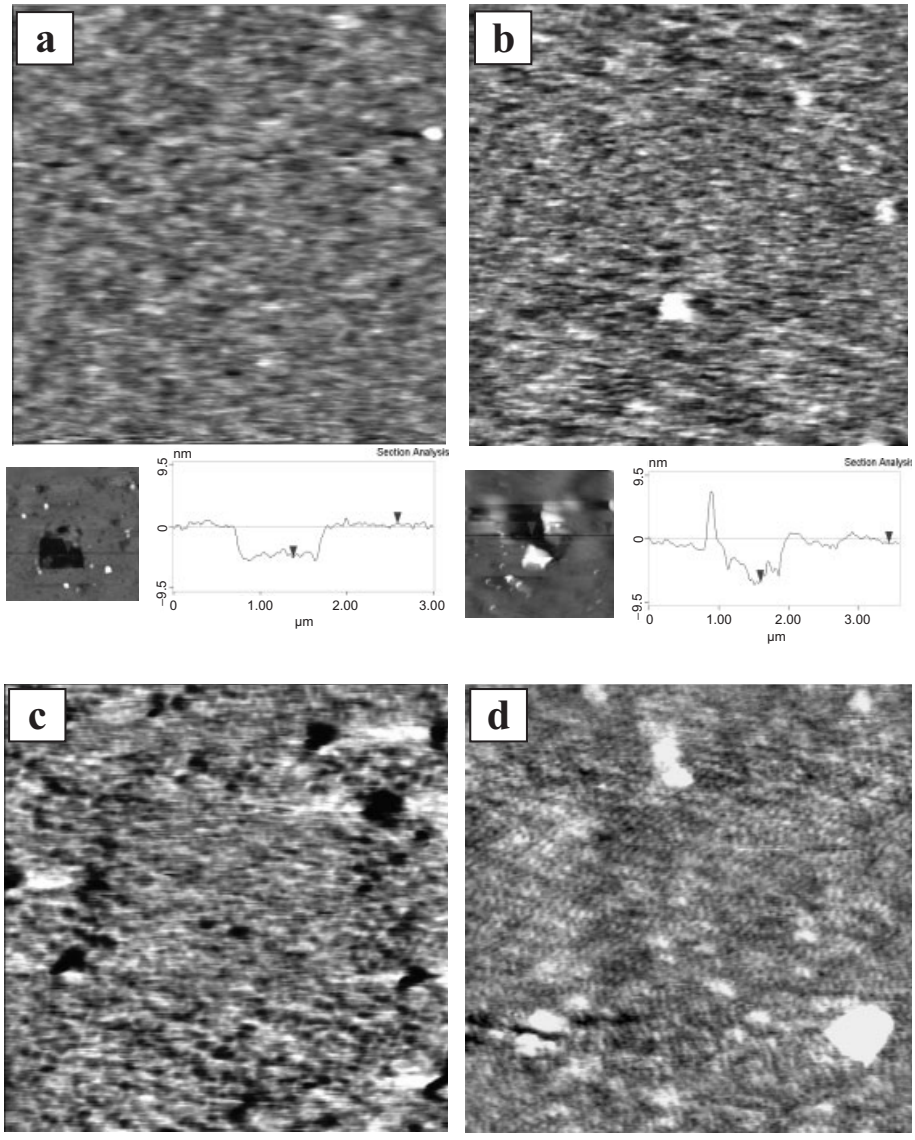

Figure 2. 1 µm×1 µm AFM topography images in fluids for **Y1** in a) toluene and b) water. Under the images are the hole produced within the layer (left) and the corresponding cross-sections used for depth measurements (right). **Y2** in c) toluene and d) water. For all images, the *Z*-scale is 5 nm.

2.2. Nanoscale Mechanical Properties

The observed conformational rearrangements should affect the mechanical properties of the brushes, and their measurement in the presence of a solvent gives a unique opportunity to assess these characteristics as a function of solvent–solute interactions (where the solvent is water or toluene) and chemical composition of the brush (**Y1** vs. **Y2**). No detectable adhesive forces were observed for either brush in toluene (Fig. 4). This, along with the repulsive nature of the FDCs, is typical for a surface of hydrophobic PS chains, which dominate the topmost surface layer. In contrast, for **Y1** in water, there was a noticeable pull-off force from the retraction curve of the FDC (Fig. 4). Typical values of this adhesion force ranged from 200 to 400 pN. This relatively high level of adhesion is expected because the hydrophilic PAA arms are extending from the surface in water, and can directly interact with the hydrophilic silicon oxide AFM tip. For **Y2**, the level of adhesion in water was even higher, with values ranging from 500 to 700 pN, which indicates strong tip–surface interactions with more PAA chains participating (Fig. 4).[22] Overall adhesives forces (normalized to the AFM-tip radius) in water were twice as large for the **Y2**-brush layer than the **Y1** layer (Table 2). This stronger adhesion with the **Y2**-brush layer in water confirms the higher effective concentration of the PAA chains on the surface of the **Y2**-brush layer (and interacting with the AFM tip) as can be expected from the volume composition of the molecules ($PAA_{\mathbf{Y1}} = 34\,\%$, $PAA_{\mathbf{Y2}} = 41\,\%$). In addition, greater probing instabilities were introduced into the topography and AFM images when scanning the asymmetric brushes (**Y1**) as compared to Y-brushes with symmetric arms (**Y2**). These instabilities were caused by the tip interacting with two very different arms (like PS and PAA) simultaneously in **Y1**.[19] This is a remarkable observation considering the fact that the phase separation

ADVANCED FUNCTIONAL MATERIALS

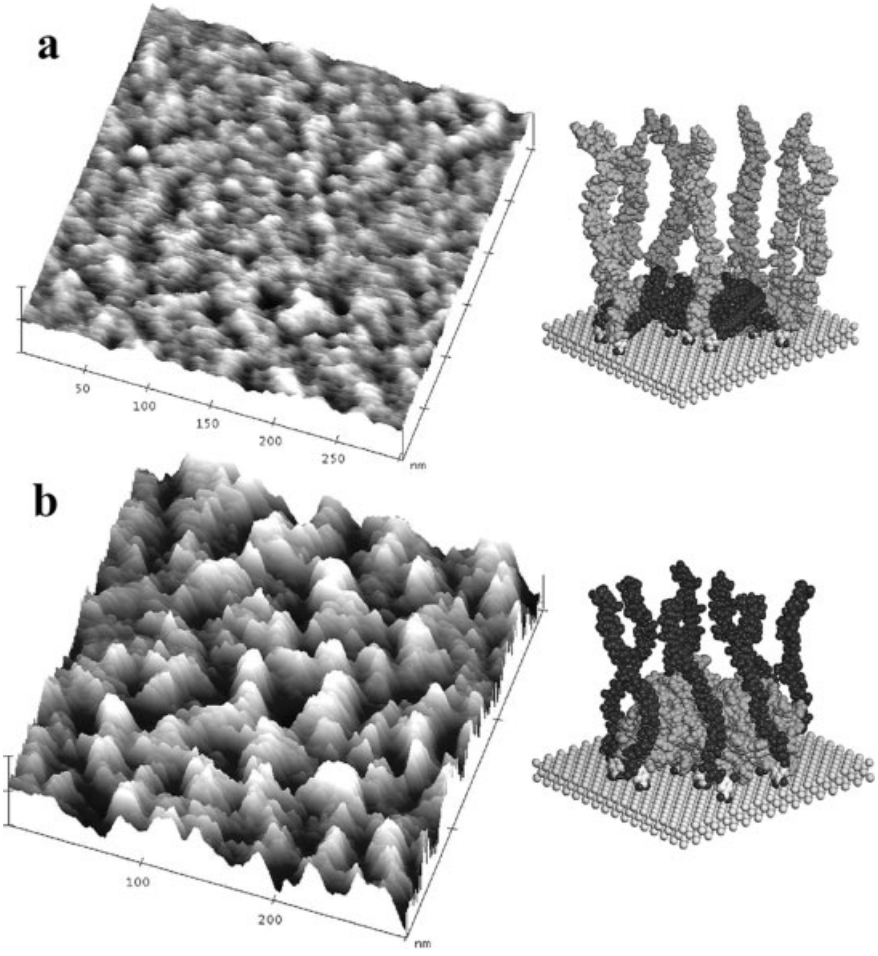

Figure 3. High-resolution (300 nm×300 nm) tapping-mode, three-dimensional AFM topography images of **Y2** in a) toluene and b) water. The corresponding molecular models are also shown.

in these brushes can only occur on the nanoscale, as it is limited by the length of the incompatible arms (≈10 nm). The sensitivity of the adhesive properties implies that small changes in chemical composition of the grafted Y-shaped molecules control the morphology in the presence of a solvent.

The nanomechanical compression properties of the brush layers in a fluid can be evaluated from load–penetration data reflecting the elastic indentation of the layers under normal load (Fig. 5). Loading curves were calculated from the FDCs using the modified, layered Hertzian model.[23,24] Penetration through the layer requires very little force below 2 nN, because the PS arms are swollen in toluene. The curves for both **Y1** and **Y2** in toluene deviate from conventional Hertzian behavior by leveling off beyond some compression owing to the presence of the stiff silicon substrate. The apparent maximum layer indentation reaches 8 nm for **Y2**, and is slightly higher for **Y1** because of the longer PS and PAA arms in **Y1**. The lines in Figure 5 are the best fit from a multilayered model based on Hertzian loading, which allows the elastic modulus and layer thickness to be evaluated.[25] An actual layer thickness derived from this analysis was close to 6 nm, which agrees well with the independent AFM scratch test in the selective solvents. The elastic modulus was less than 25 MPa for both brush layers, indicating the surface presence of swollen PS arms (Table 2).

The load–penetration curves are differently shaped in water, with the apparent indentation depth not exceeding 3 nm (Fig. 5). This change can be related to shorter PAA arms, resulting in a smaller thickness of a PAA layer over the collapsed PS phase (Fig. 3). The collapsed PS layer is impenetrable in this conformation relative to the soft AFM tip used in fluidic force measurements.

The concurrent surface mapping of topography and the elastic modulus represents a powerful tool for identifying the domain structure of brushes, and to obtain quantitative results describing their stiffness with nanoscale resolution using AFM measurements in a fluid. The topography and elastic-modulus distribution maps in Figure 6 result from taking 1024 FDCs over a 300 nm×300 nm area directly, in water, with a resolution below 10 nm. Analyzing the FDCs for **Y1** and **Y2** brushes in water with a Hertzian model, to extract the exact modulus, resulted in bimodal histograms of surface distributions for both layers (Figs. 6b,d). Both bimodal distributions obtained in fluid (water) had one peak at around 5 MPa, coming from the swollen PAA, and another peak at around 110 MPa, which is the apparent elastic modulus of the collapsed PS domains. Exact

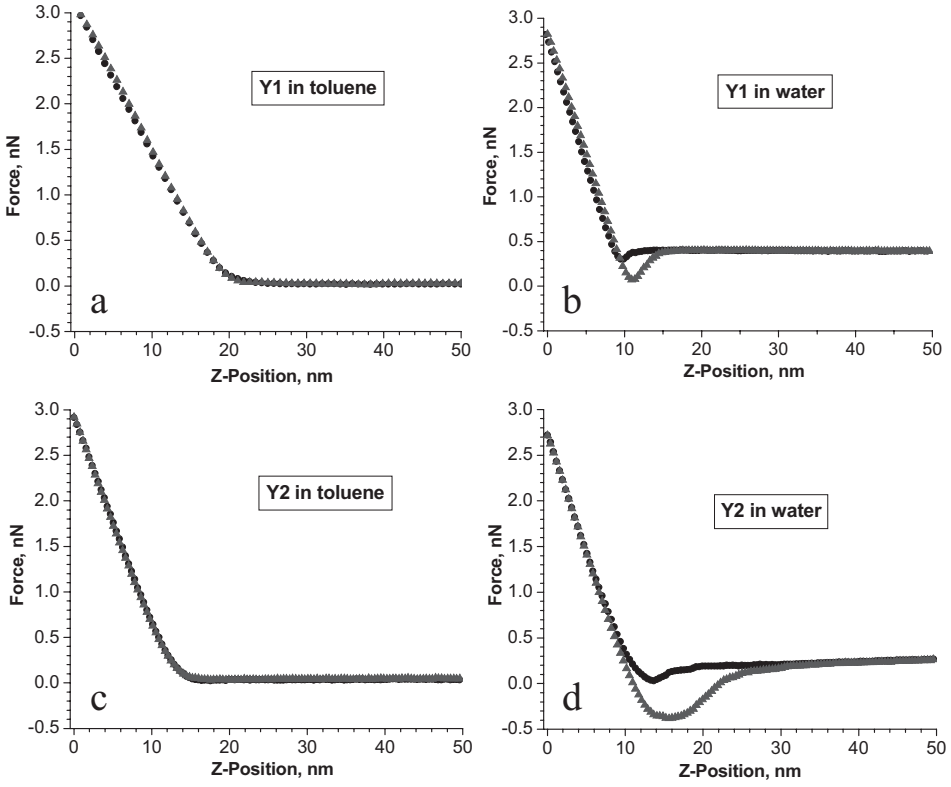

Figure 4. Representative force–distance curves (FDCs) (deflection scale converted to real force) for the Y-brushes; **Y1** in toluene (a) and water (b) and **Y2** in toluene (c) and water (d). The circles represent the approaching curve and the triangles are the retrace curve for the FDCs.

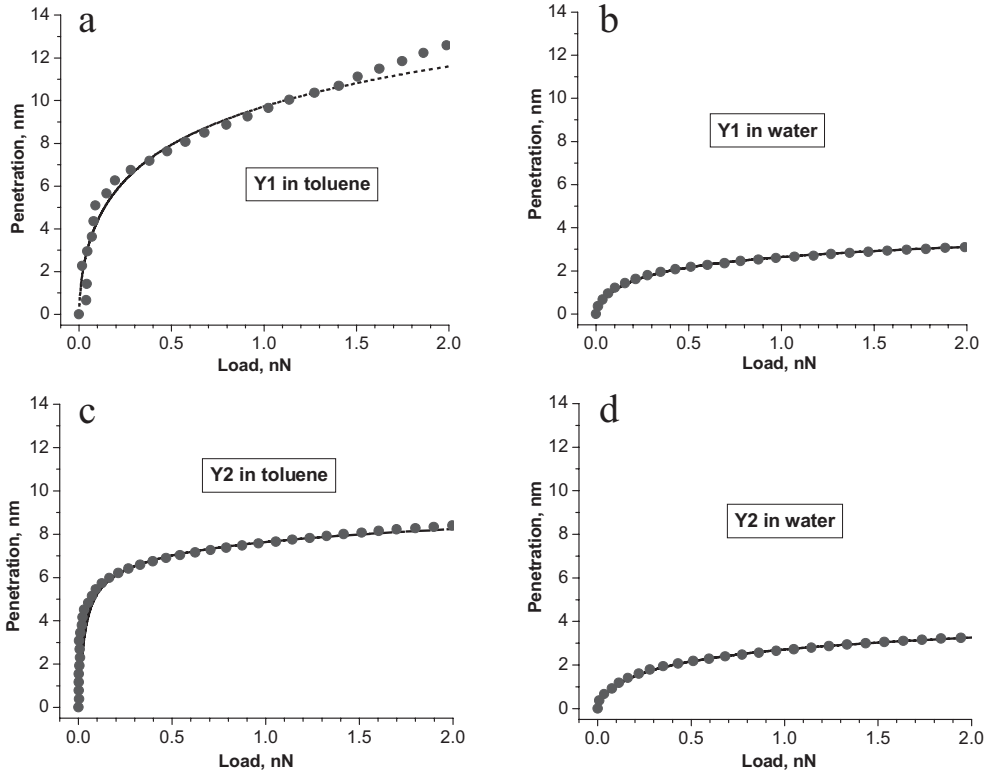

Figure 5. Representative load–penetration curves for the Y-brushes; **Y1** in toluene (a) and water (b) and **Y2** in toluene (c) and water (d). The lines in the load–penetration curves are simulated fits (see text for details).

ADVANCED FUNCTIONAL MATERIALS

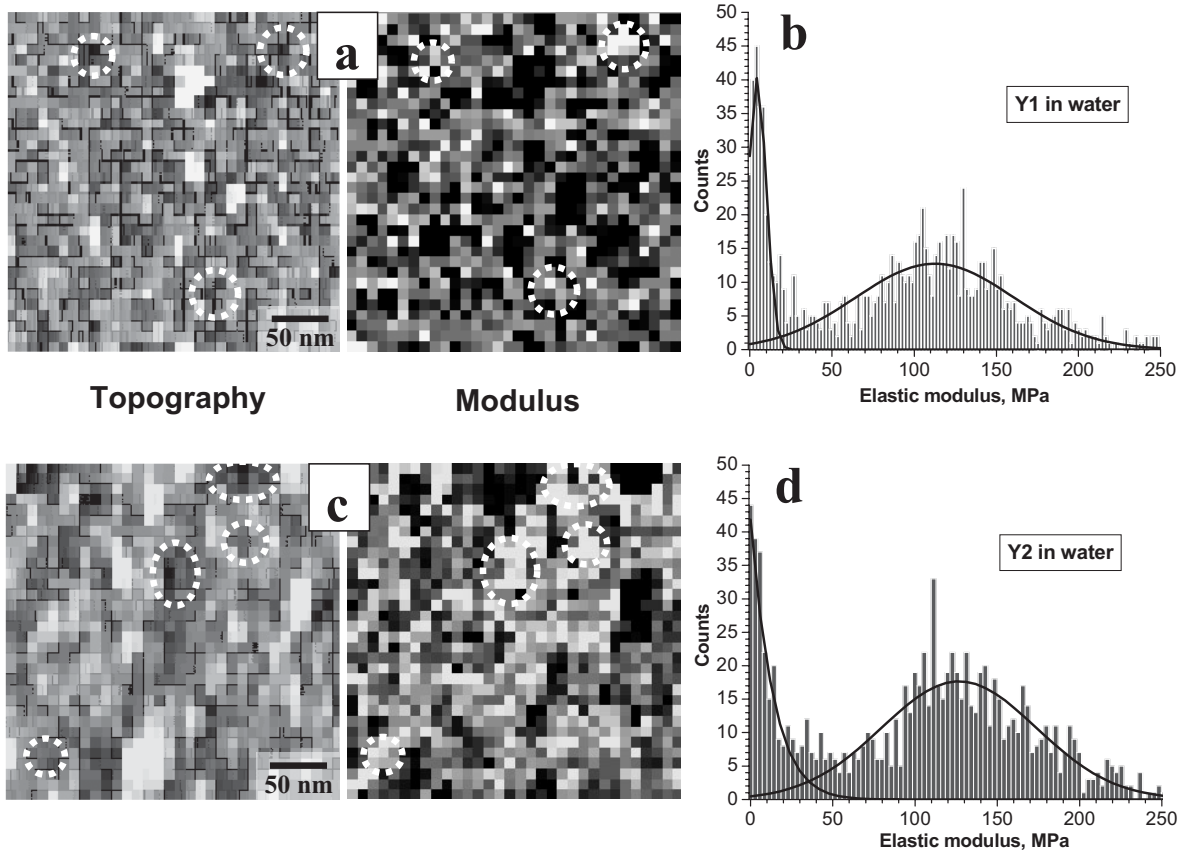

Figure 6. Simultaneous topography and force mapping over a 300 nm×300 nm area with 32×32 pixel resolution for FDCs. The resulting force–volume maps for **Y1** in water (a) gave a bimodal distribution (b) of the elastic modulus. For topography and modulus maps, the lighter the color, the higher the heights and the relative value of the modulus, respectively. The circles in the topography map indicate low points (or pits) in the topography (corresponding to collapsed PS); they correlate to the high points in the modulus map, which are indicative of hard, glassy PS chains in a bad solvent (water). The topography and modulus maps for **Y2** (c) exhibit the same behavior, also resulting in a bimodal distribution of the elastic modulus (d).

values from the Gaussian fits are given in Table 2, where the individual moduli of the "crater pit" (PS) and the "rim" (PAA) are distinguished for the water state. Close investigation of the topography and modulus maps allows one to correlate the low points in the topography (PS pits) with the high points in the elastic modulus (see circles in Figs. 6a,c). Furthermore, the high points in the topography (PAA) match the low elastic modulus values in the modulus map very closely. This force mapping confirms the presence of both arms on the surface in the water state, which leads to the higher surface roughness (Table 2).

On the other hand, the surface distribution of the elastic modulus for **Y1** and **Y2** in toluene is unimodal (deviations are within 20 %), with much lower values of the apparent elastic moduli (Figs. 7a,b). However, the most interesting observation is the five-fold increase in stiffness between **Y1** (4.6 MPa) and **Y2** (22 MPa) brushes (Table 2). This significant rise in stiffness occurs despite the fact that the volume fraction of PS only decreases from 66 to 59 %. The decreased compliance of the **Y2**-brush layer can be attributed to its shorter arms and higher grafting density, resulting in larger space constraints for arms compressed by the AFM tip. These findings clearly demonstrate that even subtle variations in the chemical composition have a profound impact on the mechanical and surface properties of switchable Y-shaped brushes in fluids. The homogeneous character of brush layers swollen in toluene indicates that the PS chains completely screen the PAA arms and form a continuous smooth surface layer over PAA, confirming our previous suggestion that was made on the basis of an initial roughness analysis and molecular modeling (Fig. 3).

2.3. Microtribological Properties of Brush Layers

The friction coefficient (μ) of **Y1** and **Y2** measured against a sliding glass ball after exposure to either toluene or water was dramatically affected by the surface composition of the layer (Fig. 8). For the **Y1**-brush layer treated with water, the friction coefficient remained stable throughout the course of the test (1000 sliding cycles) with an average value of $\mu = 0.21$ (Fig. 8a, Table 2). In contrast, the friction coefficient of **Y1** after toluene treatment is unstable and nearly twice as high as after water exposure. The same trend was also observed for **Y2**, in which the toluene-treated sample was even more unstable and total failure occurred after 700 cycles (Fig. 8b). The averaged friction coefficient of **Y2** after toluene exposure is $\mu = 0.55$, whereas

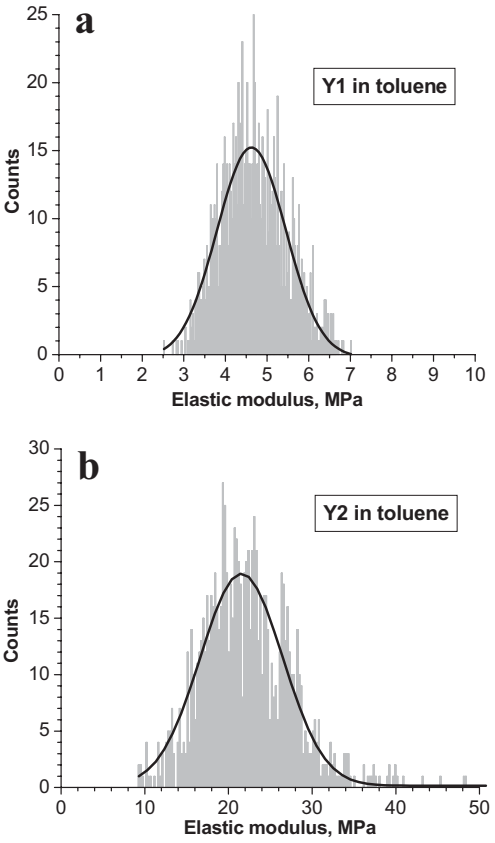

Figure 7. Surface distribution of the elastic modulus for a) **Y1** and b) **Y2** in toluene.

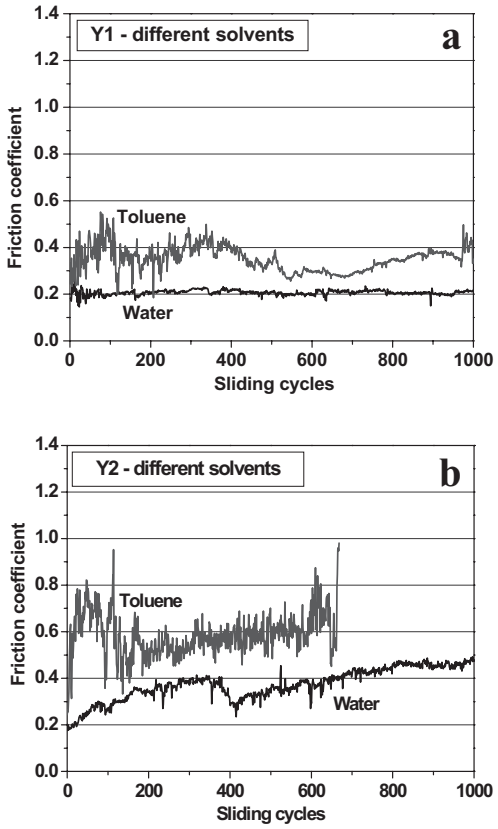

Figure 8. Microtribological data showing the friction coefficient (μ) versus the number of sliding cycles: a) **Y1** in toluene and water; b) **Y2** in toluene and water. Tests were conducted at 30% relative humidity, with a normal load of 200 μN.

after water treatment it is only 0.35 (Fig. 8b, Table 2). Note that although the absolute values of the friction coefficient for the brush layers studied here are higher than the usual values for polymeric and organic layers with optimized morphology (0.1 and below),[26,27] they are on a par with the friction coefficients found for many bulk glassy and rubbery polymers.[28]

The PS-dominated surface, which is hydrophobic with low surface energy, would be expected to have a lower friction coefficient than a surface with ≈60% coverage of the high-surface-energy PAA layer.[29] However, one should consider the viscoelasticity of short PS chains and their glass-transition temperature (T_g). It is well known that the T_g of high-molecular-weight PS is around 100 °C, but it starts to decrease rapidly when the molecular weight becomes lower than 20 kDa (1 Da = 1 g mol^{-1}). According to Fox and Flory,[30] the T_g of PS with number-average molecular weight (M_n) of 4100 g mol^{-1} (**Y1**) is approximately 50 °C, and it drops to nearly 40 °C when M_n = 2600 g mol^{-1} (**Y2**). In addition, the presence of the collapsed PAA chains beneath the PS chains can create conditions for increasing the contact area, thus facilitating higher friction forces. On the other hand, even a small amount of toluene trapped in these brushes may further decrease the T_g of the PS arms (samples dried at room temperature without annealing can contain residual solvent). However, considering that the friction coefficient is also significantly higher than that measured for PS homobrushes with similar chain lengths and measured under identical conditions (0.3–0.4),[8d] we can exclude solvent effects on Y-brush behavior and suggest a significant contribution from the junction point and PAA presence in lowering the T_g. Therefore, we suggest that the PS chains in the **Y1**, and especially the **Y2**, brushes may be above their T_g and possess an appreciable amount of segmental mobility and viscoelastic properties in the contact area under significant shear stress. As a result, a notable dissipation of energy would occur in these layers, which would explain the high friction coefficients observed. This hypothesis would be consistent with the experimental data that sliding over the **Y2** brush with shorter PS chains (lower T_g) generates greater frictional forces than in the **Y1** sample (Table 2).

The difference in friction and adhesive properties also translates to a significant difference in the wear stability of brush layers with different compositions. This difference manifests itself as a different chemical composition and surface morphology of the initial and worn surface areas. Figure 9 presents Auger electron spectroscopy (AES) depth profiles of the chemical composition in the **Y1**- and **Y2**-brush layers before and after the wear tests (after exposure to water). Apparently, molecules with shorter arms (**Y2**) experienced a very large loss of polymeric material, which was indicated by a decrease in the carbon content and an increase in the silicon signal, indicating

ADVANCED FUNCTIONAL MATERIALS

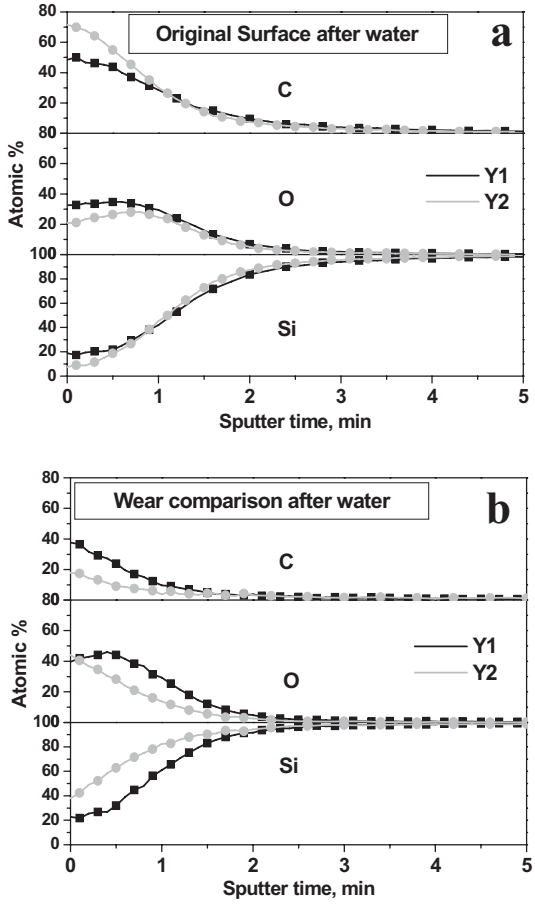

Figure 9. AES concentration profiles comparing the wear of **Y1** and **Y2** after water exposure: a) the original surface and b) the worn area.

the removal of the organic material and exposure of the underlying silicon oxide layer and silicon particles in the worn area (Figs. 9a,b). This is a result of the lower molecular weight and depressed T_g of the top layer, which still has a large PS volume fraction. The abrasion resistance of the **Y2** brush was also significantly lower.

The lower friction coefficient of PAA-enriched surfaces is a surprising result considering that these surfaces show much higher adhesion against hydrophilic glass and tip surfaces with silicon dioxide composition. Classical theories of sliding contact mechanics and experimental results have led researchers to believe that generally stiff hydrophobic surfaces should exhibit the best tribological properties.[28,31] However, very recent work shows that at the micro- and nanoscale, these theories break down because micro- and nanoscale contacts are dominated by capillary forces.[32] Water molecules adsorb on any surface exposed to air, becoming confined in these contacts. This thin layer (several monolayers, depending on the humidity) is known to reduce friction, because it acts as a lubrication layer and can prevent direct solid contact with the surface. Ahn and co-workers showed that the friction coefficient of a *hydrophilic* surface *decreased* with increasing humidity and even exhibited better tribological properties than more hydrophobic surfaces.[32] We suggest that for both the **Y1**- and **Y2**-brush layers studied here, the low friction response after water exposure is caused by the presence of a thicker water film covering the glassy PAA, which is the topmost layer. With a PAA-dominated surface possessing high water affinity, a more complete water layer forms. On the other hand, unlike PS chains (for which T_g scales with M_n), for PAA chains with the low molecular weight studied here, the T_g still remains very high, close to 97 °C.[33] Therefore, after treatment with water, a *glassy* PAA phase predominantly occupies the topmost surface layer reducing the contact area and, thus, friction forces.

The data presented in Figure 10 further support this suggestion. The **Y1**-brush layer, after water exposure, has a lower coefficient of friction at 80 % RH compared to that at 30 % RH (Fig. 10a). The wear properties, based on the AES depth profiles of chemical composition, are also better at 80 % RH. Compared to an original untested surface, the surface tested at 80 % RH showed no decrease in carbon content, whereas the surface tested at 30 % RH had a substantial loss of carbon content in the layer (Fig. 10b), which is evidence of removal of polymer from the sliding area. AES also detected more oxygen on the surface tested at 30% RH, implying partial oxidation of the worn polymeric layer (Fig. 10b).

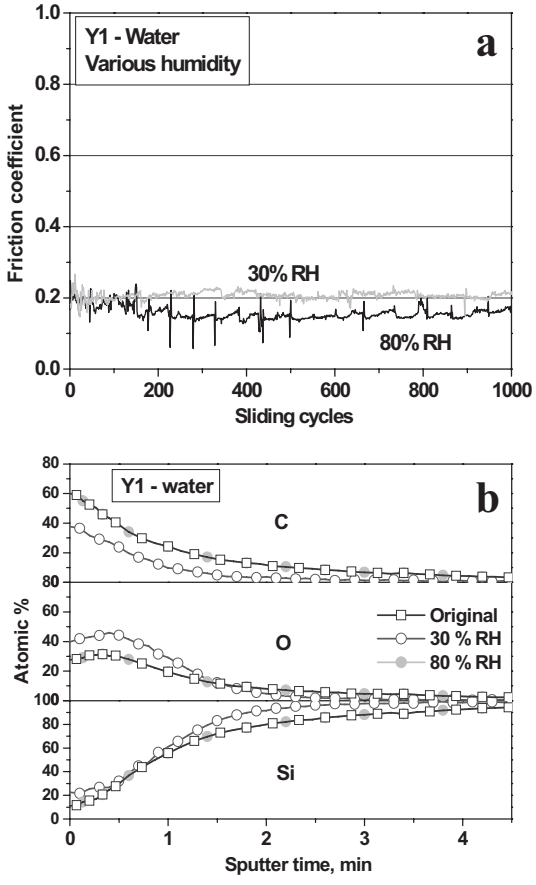

Figure 10. Data showing the effect of humidity on the microtribological properties. a) Friction coefficient as a function of sliding cycles for **Y1**; comparing results at 30 and 80 % RH. b) AES depth profiles reveal the higher material loss (in the form of less carbon for these polymeric materials) at 30 % RH, compared to an original (untested) portion of the **Y1** brush.

Finally, we compared the wear behavior of the **Y1-**brush layer after water and toluene exposure. Scanning electron microscopy (SEM) images of the wear tracks show a striking contrast between the different states (Figs. 11a,d). After water exposure, there is very little visible damage to the surface in the sliding area. However, after toluene exposure, there is significant damage to the brush layer after testing under the same conditions, clearly visible in the SEM image (Fig. 11d). The composition profiles comparing the initial and worn surfaces after water (Figs. 11b,c) and toluene exposure (Figs. 11e,f) are consistent with the SEM data. A much greater depletion of the carbon for the toluene-treated brushes, along with an increased silicon signal observed at low sputtering times, indicates nearly complete removal of the brush layer treated in toluene. After switching of a brush layer to water treatment, a significant fraction of carbon is preserved within the worn area under similar conditions despite some visible wearing (Fig. 11c). Obviously, the switching of morphology and chain reorganization in response to different solvents also correlates to changes in frictional behavior of the layer, an encouraging result for prospective nanoelectromechanical systems (NEMS) in which the frictional behavior can be tuned in fluidic surroundings.

3. Conclusions

We have characterized the morphology and nanomechanical properties of Y-shaped amphiphilic brushes in fluids as a function of chemical composition, and have measured, for the first time, their tribological characteristics. AFM-based nanomecha-

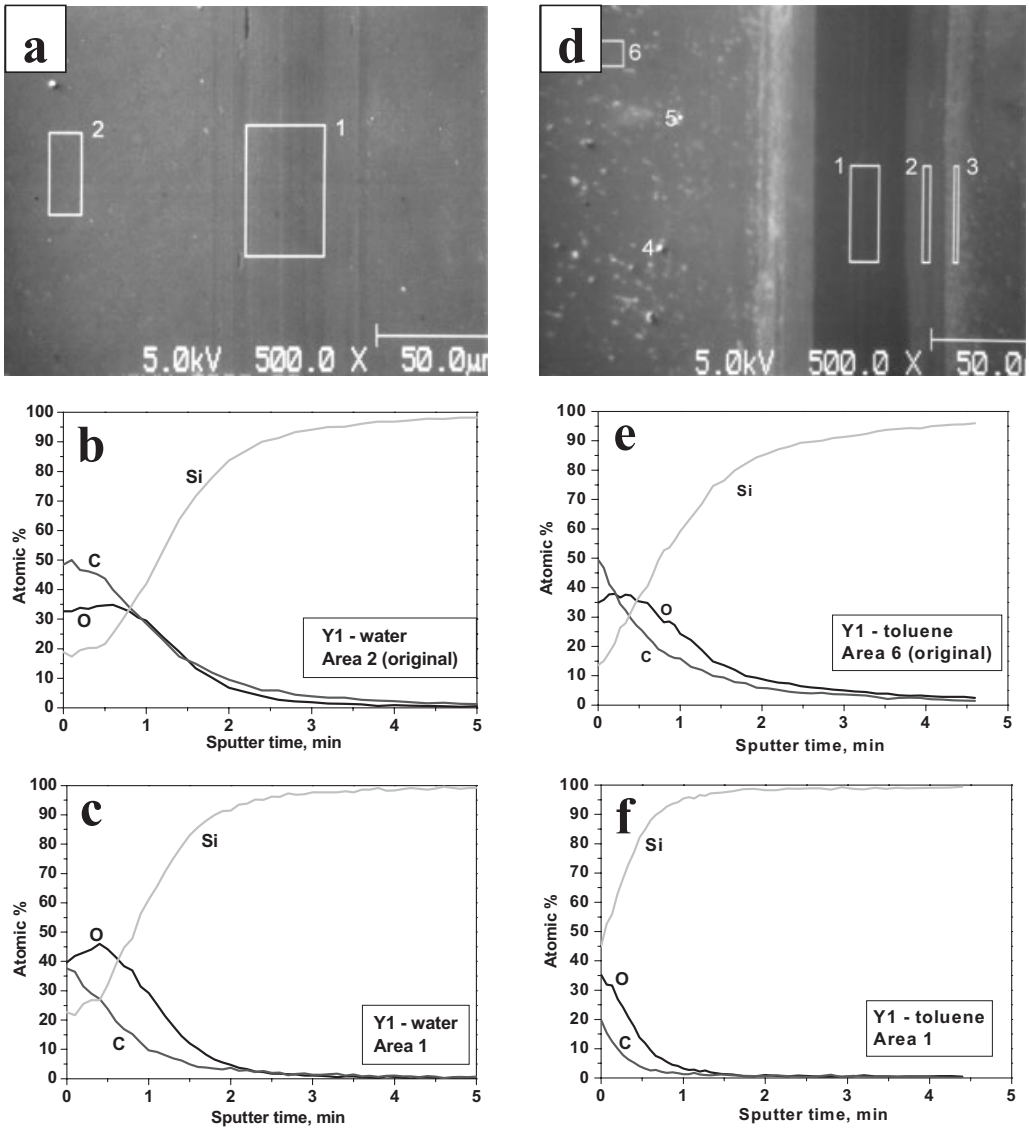

Figure 11. SEM images of the wear tracks from the microtribometer after testing **Y1** in water (a) and toluene (d). In (a), Area 2 represents the accompanying AES analysis (b) of the original non-tested surface; area 1 is where the analysis of the worn area was taken from (c). For (d), the AES analysis from the original area (e) corresponds to area 6; the worn area analyzed in (f) represents area 1 in the SEM image.

nical testing has shown that nanoscale reorganization greatly impacts the adhesion and elastic properties of the surface layer. This led to a bimodal distribution of the elastic modulus in water, which was controlled by the relative amounts of PS and PAA on the surface. On the other hand, nanomechanical probing of the surface in toluene revealed a top layer completely dominated by PS. As a result of this reorganization, which agreed well with the molecular simulations, the Y-shaped brush exhibited a variation in friction and wear properties after exposure to different solvents. Unexpectedly, the microtribological properties were enhanced for a hydrophilic, PAA-dominated surface, which showed a low friction coefficient and higher wear stability, despite its higher adhesion and heterogeneous surface composition. We suggest that this unusual behavior is caused by a combination of the presence of thicker water layers on/within the PAA-enriched surface that act as a boundary lubricant and the glassy state of the PAA chains in the dry state.

4. Experimental

The chemical structures of the synthesized Y-shaped molecules **Y1** and **Y2** are presented in Figure 1, and the fabrication of chemically grafted layers is described in detail elsewhere [17,18]. The Y-shaped brushes have one PS arm, which is the hydrophobic component, and one PAA arm, which is hydrophilic, with a varying number of monomeric units. **Y1** has an asymmetric composition with longer chains (PS_{40}-PAA_{30}); **Y2** is a symmetrical molecule (PS_{25}-PAA_{25}), as verified by NMR spectroscopy [18]. The Y-shaped molecules were attached to a functional stem-like segment that is capable of covalent grafting to a functionalized silicon surface. The polymers were spin-coated from a 1.5 wt.-% toluene solution onto the silicon wafers functionalized with epoxysilane self-assembled monolayers [34]. The coated wafers were annealed at grafting temperatures ranging from 120 °C to 150 °C for 6 h to enable the end groups to graft to the substrate. The initial microroughness of the functionalized wafers did not exceed 0.2 nm within a 1 μm × 1μm surface area. Post-grafting hydrolysis of poly(*t*-butyl acrylate) arms imparted amphiphilicity to the brush. Molecular models and simulations were carried out using Materials Studio [18]. To switch the brushes, samples were immersed in good solvents for at least 12 h to ensure full chain reorganization, as verified in our previous study on switching kinetics [19]. Toluene and water were used as good solvents for PS and PAA, respectively.

AFM studies in tapping mode under fluid were performed on a MultiMode (Nanoscope IIIa) microscope (Veeco Metrology) equipped with a fluid cell, according to procedures adapted in our lab [35]. The fluid cell was modified with fluoro-elastomer tubing that would neither dissolve in organic solvents nor deposit any contamination on the sample. Probing of the surface nanomechanical properties was conducted directly in fluids (after allowing for equilibration with solvents) using the force spectroscopy approach described previously [25]. FDCs were obtained using the force–volume mode in 32 × 32 pixel arrays within 300 nm × 300 nm surface areas. The samples were scanned in tapping mode before and after force measurements to ensure that no contamination, plastic deformation, or physical damage occurred during the application of force. The data processing and calculation of the elastic modulus from the surface distributions of over 1000 FDCs were carried out in accordance with the multilayered Hertzian contact mechanics model described earlier [25,36]. For quantitative results, great care was taken to analyze the AFM tip characteristics. We used V-shaped cantilevers with a normal spring constant measured to be 0.06—0.1 $N\,m^{-1}$ [37]. The tip profile and radius (around 20 nm) were monitored by scanning a gold nanoparticle calibration standard [38]. The sensitivity of the system was measured before and after force measurements to ensure stability.

For microtribology studies, a custom-built microtribometer, effectively an oscillation friction and wear tester [39], was used to evaluate the frictional characteristics and to study the wear resistance of the Y-shaped brushes after treatment with the selective solvents. Before testing, the brushes were "switched" by exposure to the particular solvent for 12 h, dried in ambient air under room temperature for 5 min, and immediately tested in the dry state. We used a 3 mm diameter glass ball (microroughness less than 1 nm) as the sliding counterpart over the stationary sample. The ball was ultrasonically cleaned in acetone and methanol for 30 min and dried with nitrogen prior to tests. The glass ball, mounted in a carrier head, was oscillated with an applied normal load of 200 μN, which corresponded to a maximum Hertzian pressure of 34.3 MPa. The sliding speed was 330 $\mu m\,s^{-1}$ and the stroke length was 1.6 mm. The tests were conducted in a humidity-controlled chamber at 5, 30, and 80 % RH. The chemical composition of the surfaces was probed by AES on a PHI-670 instrument. AES surface analyses were performed using a field-emission gun with an accelerating voltage of 5 kV and a current of 0.0185 μA. The working potential for depth sputtering was 1 kV using Ar ions. Under these working conditions, the sputtering rate was 7 $Å\,min^{-1}$ when calibrated against SiO_2.

Received: February 2, 2005
Final version: April 4, 2005
Published online: July 21, 2005

[1] a) *Polymer Brushes* (Eds: R. C. Advincula, W. J. Brittain, K. C. Caster, J. Rühe), Wiley-VCH, Weinheim, Germany **2004**. b) B. Zhao, W. J. Brittain, *Prog. Polym. Sci.* **2000**, *25*, 677. c) B. Zhao, W. J. Brittain, W. Zhou, S. Z. D. Cheng, *J. Am. Chem. Soc.* **2000**, *122*, 2407. d) I. Luzinov, S. Minko, V. V. Tsukruk, *Prog. Polym. Sci.* **2004**, *29*, 635. e) A. Halperin, M. Tirrell, T. P. Lodge, *Adv. Polym. Sci.* **1992**, *100*, 31. f) T. P. Russell, *Science* **2002**, *297*, 964.

[2] a) G. S. Grest, M. Murat, *Macromolecules* **1993**, *26*, 3108. b) V. Koutsos, E. W. van der Vegte, G. Hadziioannou, *Macromolecules* **1999**, *32*, 1233. c) X. Guo, A. Weiss, M. Balluff, *Macromolecules* **1999**, *32*, 6043.

[3] Y. Ito, Y. Ochiai, Y. S. Park, Y. Imanishi, *J. Am. Chem. Soc.* **1997**, *119*, 1619.

[4] a) M. E. Harmon, D. Kuckling, C. W. Frank, *Langmuir* **2003**, *19*, 10 660. b) B. Yang, W. Yang, *J. Membr. Science* **2003**, *218*, 247. c) H. Tu, C. E. Heitzman, P. V. Braun, *Langmuir* **2004**, *20*, 8313.

[5] M. Lee, J.-W. Kim, Y.-S. Yoo, S. Peleshanko, K. Larson, D. Vaknin, S. Markutsya, V. V. Tsukruk, *J. Am. Chem. Soc.* **2002**, *124*, 9121.

[6] a) M. Irie, *Adv. Polym. Sci.* **1990**, *94*, 27. b) L. Ionov, M. Stamm, S. Minko, F. Hoffmann, T. Wolff, *Macromol. Symp.* **2004**, *210*, 229.

[7] a) B. Zhao, W. J. Brittain, *Macromolecules* **2000**, *33*, 8813. b) J.-B. Kim, W. Huang, M. L. Bruening, G. L. Baker, *Macromolecules* **2002**, *35*, 5410. c) E. B. Zhulina, C. Singh, A. C. Balazs, *Macromolecules* **1996**, *29*, 8254.

[8] a) A. Sidorenko, S. Minko, K. Schenk-Meuser, H. Duschner, M. Stamm, *Langmuir* **1999**, *15*, 8349. b) S. Minko, S. Patil, V. Datsyuk, F. Simon, K. J. Eichorn, M. Motornov, D. Usov, I. Tokarev, M. Stamm, *Langmuir* **2002**, *18*, 289. c) M. LeMieux, D. Usov, S. Minko, M. Stamm, H. Shulha, V. V. Tsukruk, *Macromolecules* **2003**, *36*, 7244. d) M. C. LeMieux, D. Julthongpiput, K. N. Bergman, P. D. Cuong, H.-S. Ahn, Y.-H. Lin, V. V. Tsukruk, *Langmuir* **2004**, *20*, 10 046.

[9] a) M. Motornov, S. Minko, K. J. Eichorn, M. Nitschke, F. Simon, M. Stamm, *Langmuir* **2003**, *19*, 8077. b) J.-F. Joanny, *Langmuir* **1992**, *8*, 989. c) J. Klein, Y. Kamiyama, H. Yoshizawa, J. N. Israelachvili, G. H. Fredrickson, P. Pincus, L. J. Fetters, *Macromolecules* **1993**, *26*, 5552. d) L. Léger, E. Raphaël, H. Hervet, *Adv. Polym. Sci.* **1999**, *138*, 186. e) T. Kreer, M. H. Muser, *Wear* **2003**, *25*, 827.

[10] a) S. T. Milner, *Science* **1991**, *251*, 905. b) A. C. Balazs, C. Singh, E. Zhulina, S.-S. Chern, Y. Lyatskaya, G. Pickett, *Prog. Polym. Sci.* **1997**, *55*, 181. c) B. Zhao, W. J. Brittain, *Macromolecules* **2000**, *33*, 342.

[11] J. F. Marko, T. A. Witten, *Phys. Rev. Lett.* **1991**, *66*, 1541.

[12] a) B. Zhao, *Langmuir* **2004**, *20*, 11 748. b) B. Zhao, R. T. Haasch, S. MacLaren, *Polymer* **2004**, *45*, 7979.

[13] a) S. Minko, M. Müller, D. Usov, A. Scholl, C. Froeck, M. Stamm, *Phys. Rev. Lett.* **2002**, *88*, 035 502. b) M. Müller, *Phys. Rev. E* **2002**, *65*, 030802. c) G. E. Yakubov, B. Loppinet, H. Zhang, J. Rühe, R. Sigel, G. Fytas, *Phys. Rev. Lett.* **2004**, *92*, 115 501.
[14] M. O. Gallyamov, B. Tartsch, A. R. Khokhlov, S. S. Sheiko, H. G. Börner, K. Matyjaszewski, M. Möller, *Chem. Eur. J.* **2004**, *10*, 4599.
[15] a) C. Singh, A. C. Balazs, *Macromolecules* **1996**, *29*, 8904. b) E. B. Zhulina, A. C. Balazs, *Macromolecules* **1996**, *29*, 2667.
[16] A. Stamouli, E. Pelletier, V. Koutsos, E. van der Vegte, G. Hadziioannou, *Langmuir* **1996**, *12*, 3221.
[17] J. Teng, E. R. Zubarev, *J. Am. Chem. Soc.* **2003**, *125*, 11 840.
[18] D. Julthongpiput, Y.-H. Lin, J. Teng, E. R. Zubarev, V. V. Tsukruk, *Langmuir* **2003**, *19*, 7832.
[19] D. Julthongpiput, Y.-H. Lin, J. Teng, E. R. Zubarev, V. V. Tsukruk, *J. Am. Chem. Soc.* **2003**, *125*, 15 912.
[20] Y.-H. Lin, J. Teng, E. R. Zubarev, H. Shulha, V. V. Tsukruk, *Nano Lett.* **2005**, *5*, 491.
[21] S. Alexander, *J. Phys.* **1977**, *38*, 977.
[22] W. Zhang, X. Zhang, *Prog. Polym. Sci.* **2003**, *28*, 1271.
[23] Z. Huang, S. A. Chizhik, V. V. Gorbunov, *J. Mater. Sci.* **1998**, *33*, 4905.
[24] H. Shulha, A. Kovalev, N. Myshkin, V. V. Tsukruk, *Eur. Polym. J.* **2004**, *40*, 949.
[25] A. Kovalev, H. Shulha, M. LeMieux, N. Myshkin, V. V. Tsukruk, *J. Mater. Res.* **2004**, *19*, 716.
[26] V. V. Tsukruk, *Adv. Mater.* **2001**, *13*, 95.
[27] A. Sidorenko, H.-S. Ahn, D.-I. Kim, H. Yang, V. V. Tsukruk, *Wear* **2002**, *252*, 946.
[28] *Microstructure and Microtribology of Polymer Surfaces* (Eds. V. V. Tsukruk, K. Wahl), ACS Symposium Series, vol. 741, ACS, Washington, DC, **2000**.
[29] *Fundamentals of Friction: Macroscopic and Microscopic Processes* (Eds: I. L. Singer, H. M. Pollack), Kluwer Academic, Boston, MA **1992**.
[30] T. G. Fox, P. J. Flory, *J. Chem. Phys.* **1950**, *21*, 581.
[31] H. Ahn, D. Julthongpiput, D.-I. Kim, V. V. Tsukruk, *Wear* **2003**, *255*, 801.
[32] D. I. Kim, H. S. Ahn, D. H. Choi, *Appl. Phys. Lett.* **2004**, *84*, 1919.
[33] J. M. G. Cowie, I. J. McEwen, M. T. Garay, *Eur. Polym. J.* **1987**, *23*, 917.
[34] I. Luzinov, D. Julthongpiput, A. Liebmann-Vinson, T. Cregger, M. D. Foster, V. V. Tsukruk, *Langmuir* **2000**, *16*, 504.
[35] V. V. Tsukruk, *Rubber Chem. Technol.* **1997**, *70*, 430.
[36] V. V. Tsukruk, A. Sidorenko, V. V. Gorbunov, S. A. Chizhik, *Langmuir* **2001**, *17*, 6715.
[37] J. L. Hazel, V. V. Tsukruk, *Thin Solid Films* **1999**, *339*, 249.
[38] a) V. V. Tsukruk, V. Gorbunov, *Microsc. Today* **2001**, *1*, 8. b) M. Radmacher, R. W. Tillmann, H. E. Gaub, *Biophys. J.* **1993**, *64*, 735.
[39] D. Julthongpiput, H. Ahn, D. Kim, V. V. Tsukruk, *Tribol. Lett.* **2002**, *13*, 35.

